Numerical fault simulation in Himalayas with 2 D finite element method

M. Farhad Howladar and Daigoro Hayashi

Department of Physics and Earth Sciences, University of the Ryukyus, Nishihara, Okinawa 903-0213

Abstract: The nature of the stress field in the Himalaya is examined by the 2 D finite element method where linear elastic rheology and plain strain condition are assumed. The Mohr-Coulomb failure criterion has been adopted to analyze the relationship between stress distribution and fault formation. Two profile models are prepared and convergent displacement is imposed on them along the NE-SW horizontal direction. The convergent displacement and physical properties of the rock layer control the distribution, orientation, magnitude and intensity of the stress and fault development. According to the calculated stress pattern, thrust faults are expected to develop in the central Himalaya (model A). Normal and some thrust faults take place in the north-western Himalaya (model B). The results from our numerical experiment are in agreement with those from the seismicity and focal mechanism solution of earthquakes and also with those of M.M. Alam and D. Hayashi (Bull. Fac. Sci. Univ. Ryukyus, **73**, 15, 2002) in the central Himalaya.

key words: numerical simulation, fault, Himalaya, finite element method

1. Introduction

The Himalayan mountain range (Fig. 1) is a long and wide mountain belt which is attributed to the collision of two supreme continents (Dèzes, 1999). For this reason, the Himalayan mountain belt has been investigated by many earth scientists, including geologists, geochemists, climatologists and so on. There are many unclear problems in the Himalaya. For example active steep faults close to the Main Boundary Thrust (MBT) are normal faults in a dynamically compressional wedge (Mugnier *et al.,* 1994) where thrust faults are expected from Anderson theory (1951). The major active fault along the Himalayan range is the Main Frontal Thrust (MFT) that marks the southern edge of the Himalayan foothills (Nakata, 1989). Why are the MBT and MFT not connected but separated zones? Fault plane solutions in the Himalayan region give the same pattern of thrust faulting (Banghar, 1974). Why have the normal and thrust faults occurred?

Our aim is to analyze the stress distribution on the geological cross sections (Figs. 2A and B) in the Himalaya by the finite element method (FEM). The second aim is to specify the possible area of faults and their types by adopting the Mohr-Coulomb failure criterion.
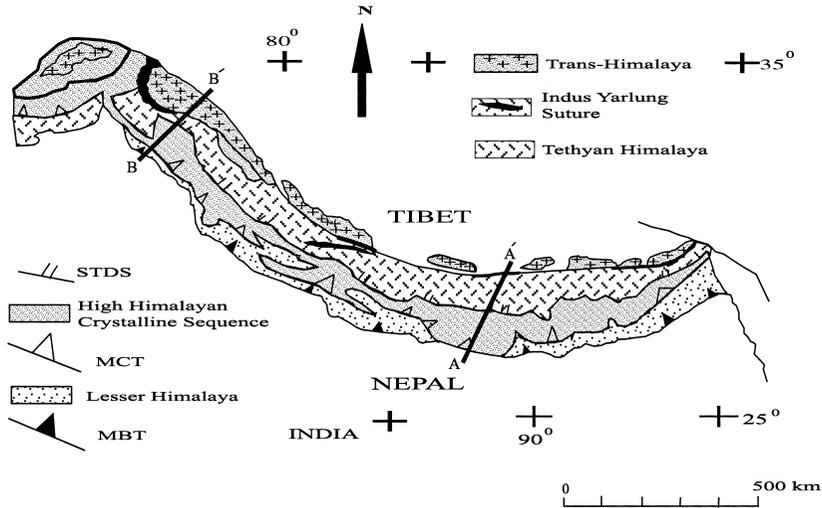
Fig. 1. Generalized geologic map of Himalayan extremity showing the main litho-tectonic units of the orogen. Slightly modified from Le Fort (1975) and Dèzes (1999).

2. Outline of geology

Two geological cross sections have been taken from different areas in the Himalaya (Fig. 2). Cross section A (Model A) is produced from the central Himalaya of Nepal after Brunel (1986) and Pandy *et al.* (1999). Section B (Model B) is produced from the north-western Himalaya after Dèzes (1999). Two sections are marked by lines A–A′ and B–B′ in Fig. 1. These are distinguished by their geological character. Summarized tectonic zones, major tectonic boundaries and brief geology of these section profiles are described as follows (Table 1).

2.1. Pre-Cambrian basement zone

Basement rocks are distributed in many places in India, south of the Himalaya. They are named Archaean Granites, Banded Gneiss Complex, Aravalli System, Delhi System and Vindhyan System from older to younger (Gansser, 1964). Although Pre-Cambrian basement rocks are not seen in the Himalayan region, we treat the Ladakh granite (Cretaceous) as a Pre-Cambrian basement in terms of its physical properties.

2.2. Sub-Himalayan zone

The Main Boundary Thrust (MBT) separates the metapsammitic schists and phyllites of the Lesser Himalaya from the conglomerates and sandstones of the Sub-Himalaya (Arita *et al.,* 1984). This steep thrust flattens with depth to develop during Pliocene time and has been shown as active through the Pleistocene (Ni and Barazangi, 1984).
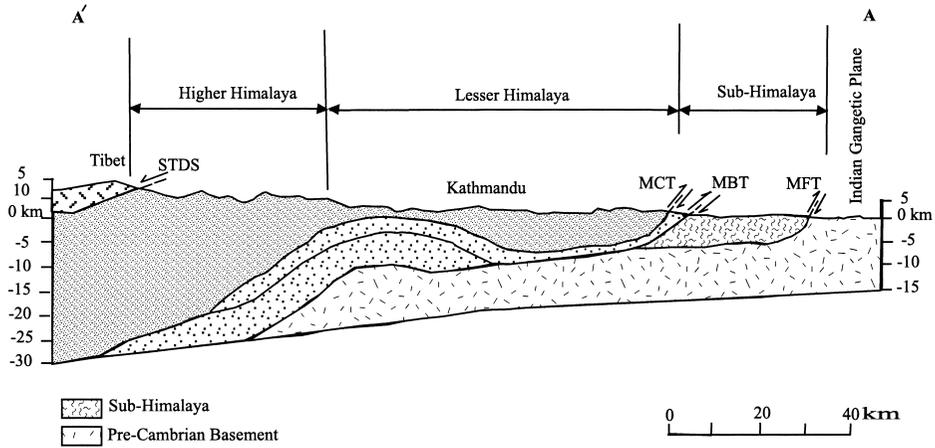
Fig. 2A.   *Geologic cross section across the central Himalaya of Nepal.   Slightly modified from Brunel (1986) and Pandey et al. (1999).*
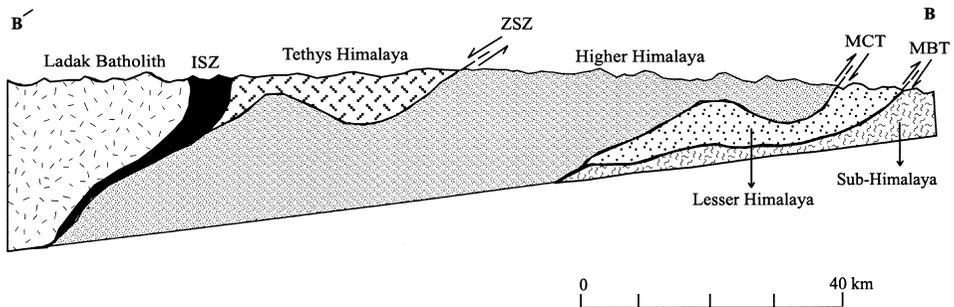
Fig. 2B.   *Geologic cross section of the north-western Himalaya, modified from Dèzes (1999).*

Table 1.   *Stratigraphic zones and Tectonic lines of the Himalaya modified after Kano (1984).*

--------------------- Indus-Tsangpo Suture Zone (ITSZ)-----------------

Tethys Himalaya

-------------South Tibetan Detachment System (STDS)--------------

Higher Himalaya

-------------------Main Central Thrust (MCT)----------------------------

Lesser Himalaya

------------------Main Boundary Thrust (MBT)------------------------

Sub-Himalaya

2.3. Lesser Himalayan zone

The Lesser Himalayan zone is bounded by the Main Central Thrust (MCT) in the north and MBT to the south.   The rock layers observed here contain various species of rocks which belong to the Midland metasediments group.   The southern facies of the group are composed of limestone, slate and phyllite; northern facies consist of slate, limestone and siliceous sandstone and with some schist (Hayashi *et al.,* 1984).

2.4. Higher Himalayan zone

The Higher Himalaya is also known as the Central Crystalline which is comprised of deformed metamorphic rocks and is marked by the axis of orogenic uplift.   Mica schist, quartzite, paragneiss, migmatite and leucogranite bodies characterize this uppermost Himalayan zone.   They represent a multiphase deformation event (Sorkhabi and Macfarlane, 1999).

2.5. Tethys Himalayan zone

The South Tibetan Detachment System (STDS) represents a major system of north-dipping structural detachments at the boundary between the Higher Himalayan crystalline sequence and the Tethys Himalaya.   The Tethys Himalayan zone is located to the south of the Indus Tsangpo Suture Zone (ITSZ) and extends from Kashmir to Nepal.   They consist of thick 10–17 km marine sediments that were deposited on the continental shelf and slope of the Indian continent.   This deposition occurred as India was drifting but still in the southern hemisphere (Verma, 1997).

3.   Simulation of fault formation

In performing the FEM analysis, we assume the linear elastic rheology and plane strain situation.   We followed the basic mathematics of Hayashi and Kizaki (1972) to construct a finite element model for elasticity.

3.1. Finite element models A and B

Models A and B are divided into triangular elements which cover the total area of all models.   Five major tectonic units are recognized as Pre-Cambrian Basement, Sub-Himalaya, Lesser Himalaya, Higher Himalaya and Tethys Himalaya.   They are named layers 1, 2, 3, 4 and 5, respectively and shown in Table 2 and Figs. 3A and B. The length and depth of models A and B are 140 km $\times$ 32 km and 290 km $\times$ 46 km, respectively.   Model A contains 479 elements and 285 nodal points.   Model B is comprised of 593 elements with 358 nodal points which are shown in Figs. 5A and B. Simulations are performed for two cases, one for calculation of the stress state shown in Fig. 6 and the other for fault formation shown in Fig. 7.

3.2. Mohr-Coulomb failure criterion

The Mohr-Coulomb failure envelope is shown in Fig. 4.   All the finite element models are in a 2 D elastic state under the plain strain condition.   Since 2 D stress fields of the numerical models are calculated with the elas. f code (developed by D. Hayashi), the third principal stress σ^* is given; it acts perpendicularly to the section plane and can

Table 2. *Structural units, considering layers and their respective major and most common rock properties.*

Structural Units	Considering Layers	Major and most common rocks
Pre-Cambrian Basement	Layer 1	Granite and gneiss
Sub-Himalaya	Layer 2	Sandstone
Lesser Himalaya	Layer 3	Metasediments
Higher Himalaya	Layer 4	Gneiss and granite
Tethys Himalaya	Layer 5	Limestone and sandstone
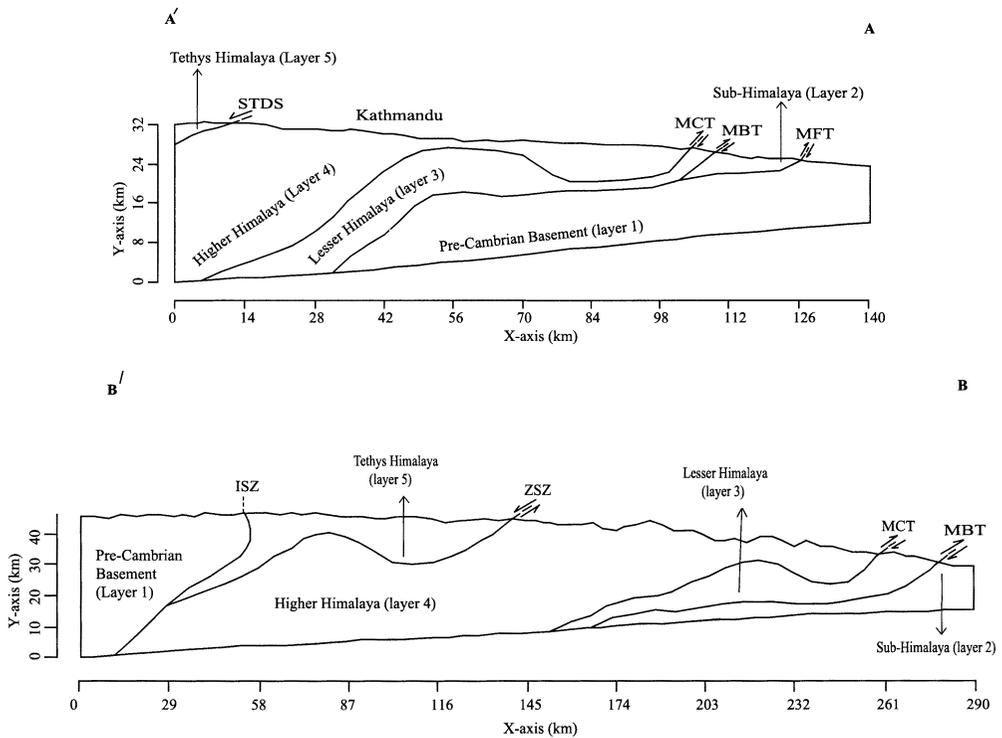
Fig. 3. *Simplified geometrical configuration of finite element models A and B. Both models represent five major structural units as their regional tectonic setting such as Pre-Cambrian Basement, Sub-Himalaya, Lesser Himalaya, Higher Himalaya and Tethys Himalaya and consider them here as layers 1, 2, 3, 4 and 5, respectively. MFT=Main Frontal Thrust, MBT=Main Boundary Thrust, MCT=Main Central Thrust, STDS=South Tibetan Detachment System, ISZ=Indus Suture Zone and ZSZ=Zanskar Shear Zone.*
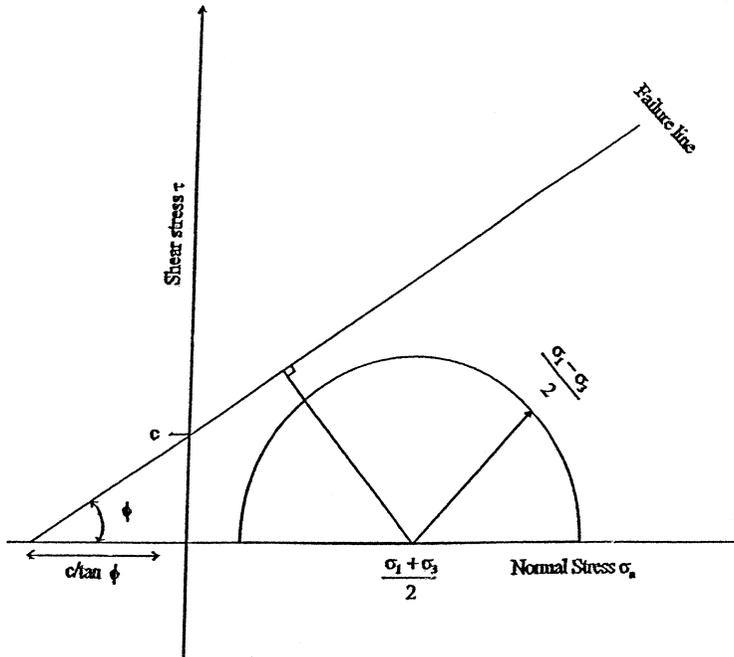
Fig. 4. *Construction of Mohr-Coulomb failure envelope demonstrating the concept of proximity to failure, after Melosh and Williams (1989). c is the cohesive strength and ϕ is the angle of internal friction.*

be obtained from the theory of plain strain as:

$$\sigma^* = \nu(\sigma_1 + \sigma_2), \tag{1}$$

where ν is Poisson's ratio (Timoshenko and Goodier, 1970; Hayashi and Kizaki, 1972). Since the values of σ_1, σ_2, and σ^* for every element have been calculated, calculation can define which are the maximum, intermediate and minimum principal stresses among them. The 2 D stress field in the plain strain state is considered as a pseudo 3 D stress field with the newly calculated principal stresses, σ_1, σ_2 and σ_3. When the whole stress field of each model is calculated, it is possible to describe in which finite element failure occurs and a fault will develop according to the Mohr-Coulomb failure criterion. The criterion is expressed on the basis of the linear relationship between the shear stress (τ) and the normal stress (σ_n)

$$\tau = c + \sigma_n \cdot \tan\phi, \tag{2}$$

where c is the cohesion of rock and ϕ is the angle of internal friction (Melosh and Williams, 1989). As a rule, failure occurs when the Mohr circle first touches the failure envelope. This takes place when the radius of the Mohr circle, $(\sigma_1 - \sigma_3)/2$ is equal to the perpendicular distance from the center of the circle at $(\sigma_1 + \sigma_3)/2$ to the failure envelope. It is possible to calculate the proximity to failure (P_f) for each element by the following equations (Melosh and Williams, 1989).

$$\left(\frac{\sigma_1-\sigma_3}{2}\right)_{\text{failure}}=c\cos\phi+\left(\frac{\sigma_1+\sigma_3}{2}\right)\sin\phi, \tag{3}$$

$$P_{\text{f}}=\left(\frac{\left(\dfrac{\sigma_1-\sigma_3}{2}\right)}{\left(\dfrac{\sigma_1-\sigma_3}{2}\right)_{\text{failure}}}\right). \tag{4}$$

Using these equations, the value of P_{f} is calculated. Whenever the value of P_{f} is less than 1.0 the Mohr circle is inside the failure envelope, which indicates that no fault occurs; on the other hand, faulting occurs if the P_{f} value is over 1.0.

3.3. Layer properties

All models are divided into five layers as shown in Figs. 3A and B with different layer properties. The dominant rocks are gneiss, granite, sandstone, metasediments and limestone, which are listed in Table 2. The physical properties of layers are defined by five parameters such as Young's modulus, Poisson's ratio, density, cohesion and angle of internal friction. Values of these parameters are listed in Table 3. The orders of strength (competence) of layers are from strong to weak. To understand clearly the order of strength of layers, we simply arrange these parameters of layers from top to bottom, which indicates the strongest layer 1 and weakest layer 2.

3.4. Boundary conditions

The characteristics of stresses are directly derived from the imposed displacement

Table 3. Layer properties that have been used in models A and B. Values of these parameters have been collected and modified from Sydney and Clark (1966).

Layer	Young's Modulus (GPa)	Poisson's Ratio	Density (kg/m^3)	Friction angle (degree)	Cohesion (MPa)
Layer 1	80	0.30	2800	45	30.00
Layer 2	40	0.20	2500	30	10.00
Layer 3	64	0.25	2680	39	20.00
Layer 4	72	0.27	2740	42	25.00
Layer 5	58	0.23	2650	37	17.50
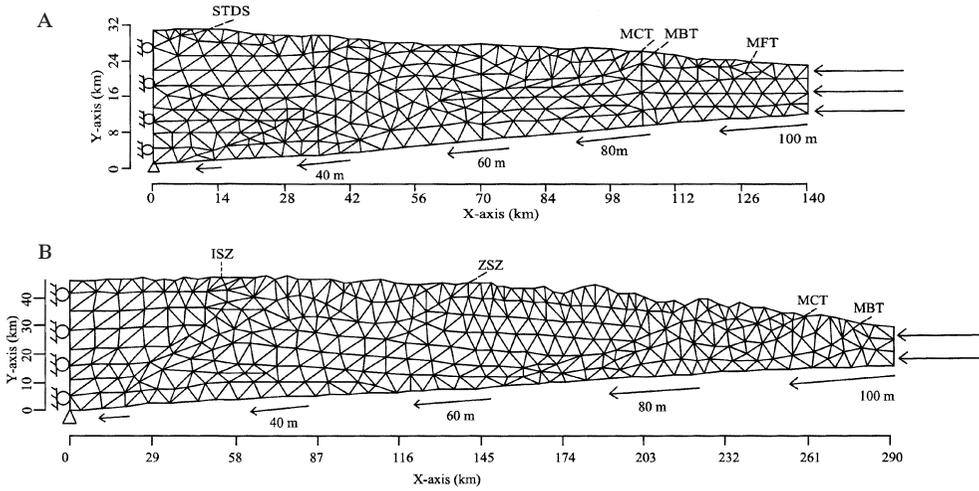
Fig. 5. Element partitions and boundary conditions of models A and B (see text for details). The
line with arrow indicates the imposed convergence displacement.

boundary conditions.   We imposed displacement boundary conditions instead of forces because the relative velocity of plate movement between the Indian subplate and Eurasian plate is known.   Since the Indian subplate is subducted beneath the Eurasian plate, the convergent displacement is perpendicular to the right boundary and the nodes at the left edge are fixed horizontally but free vertically.   The upper part of the model is a free surface.   The left bottom corner (origin) is anchored.   The gradual change of the length of line with arrow indicates that the convergent displacement increases proportionally from the origin to the right bottom corner (Figs. 5A and B).

We performed a number of simulations with different combinations of convergent displacement boundary conditions derived from the convergent velocity, e.g. 2.5 cm/yr, 3 cm/yr, 5 cm/yr, 7.5 cm/yr and 10 cm/yr along NE-SW direction.

3.5. Results of stress field

We calculate models with varying value of the layer properties in order to detect the effect of changes in stress and find that the pattern of stress only slightly sensitive to the absolute value but moderately influenced by the ratio of the layer properties.   This indicates that the model geometry and boundary conditions play more important roles than the difference of layer properties.

We determined the stress field throughout the model using the boundary conditions. The influences of boundary condition on stress field for all the simulations are nearly the same over the studied area.   Calculated stress states are shown in Figs. 6A and B for convergent displacements 100 m and 250 m, respectively.   The states of principal stress are summarized in Table 4.   The distribution of stress in every model is presented by principal stresses (σ_1 and σ_2) within the triangular domain.   The principal stresses are mostly compressive but in the upper part of the Higher Himalaya; there are some tensile stresses. σ_1 is named the maximum compressive stress and σ_2 is the minimum compres-
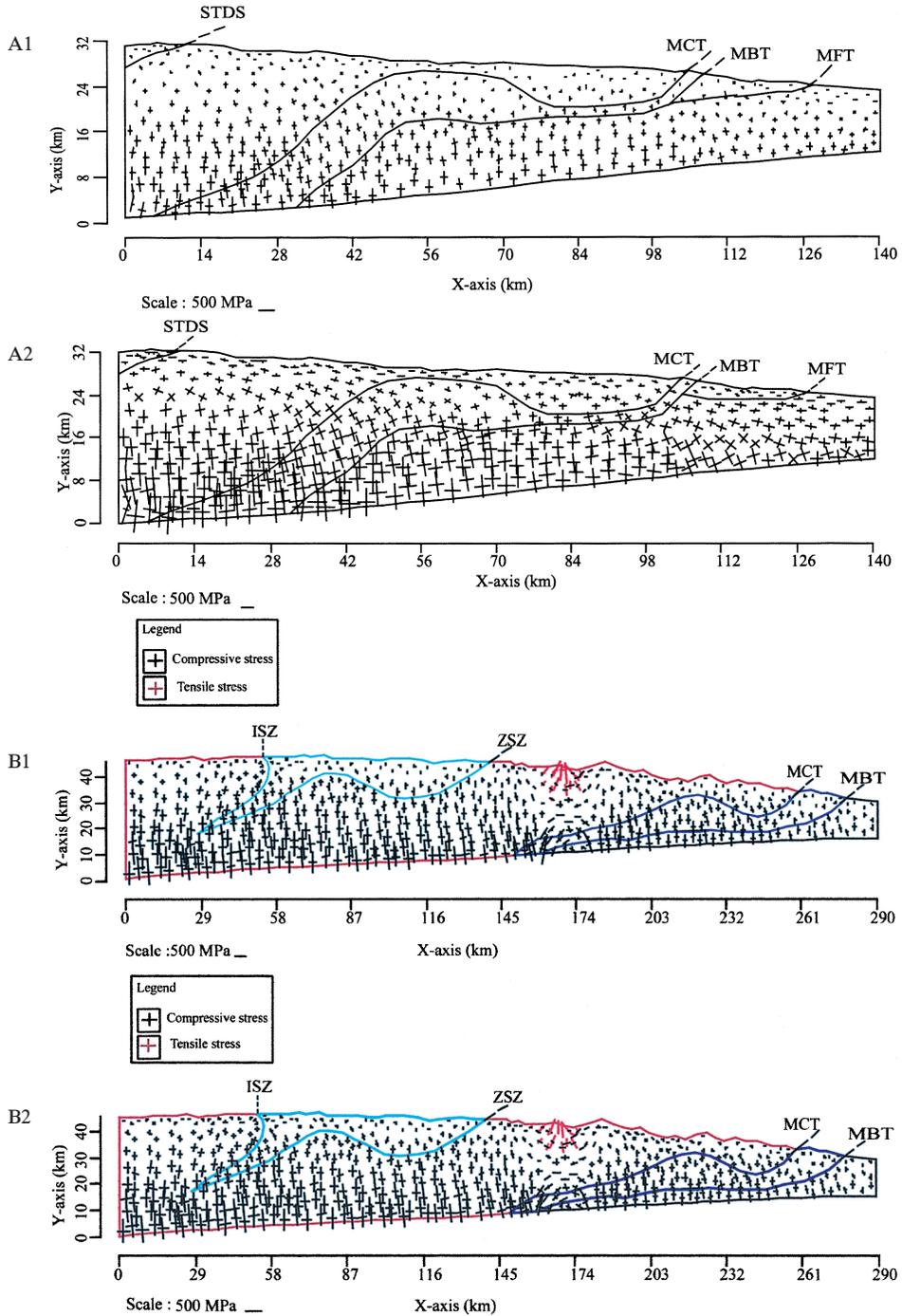
Fig. 6. *Distribution, orientation and magnitude of stresses of models A1, A2, B1 and B2 under 100 m and 250 m convergence displacements, respectively. Black color with straight line reflects compressive and red color with straight line represents the tensile stress.*

Table 4. Summarized stress state and direction of the numerically simulated models A and B. (Note: magnitudes of principal stresses are comparatively higher in the deeper part than the upper part of all experiments for both models).

Model A

Layer	Part of layer	State of stress	Direction of σ_1	Direction of σ_2
Layer 1	Upper part	Compressive	Vertical	Horizontal
	Middle part	Compressive	Inclined	Inclined
	Deeper part	Compressive	Vertical	Horizontal
Layer 2	Upper part	Compressive	Vertical	Horizontal
	Deeper part	Compressive	Vertical	Horizontal
Layer 3	Upper part	Compressive	Vertical	Horizontal
	Middle part	Compressive	Inclined	Inclined
	Deeper part	Compressive	Vertical	Horizontal
Layer 4	Upper part	Compressive	Horizontal	Vertical
	Middle part	Compressive	Inclined	Inclined
	Deeper part	Compressive	Vertical	Horizontal
Layer 5	Whole part	Compressive	Horizontal	Vertical

Model B

Layer	Part of layer	State of stress	Direction of σ_1	Direction of σ_2
Layer 1	Whole part	Compressive	Vertical	Horizontal
Layer 2	Whole part	Compressive	Vertical	Horizontal
Layer 3	Whole part	Compressive	Vertical	Horizontal
Layer 4	Upper part	Tensile	Vertical	Horizontal
	Deeper part	Compressive	Vertical	Horizontal
Layer 5	Upper part	Compressive	Horizontal	Vertical
	Deeper part	Compressive	Vertical	Horizontal

sive stress.   In every figure (Figs. 6A1, A2, B1 and B2), each pair of lines which are perpendicular to each other and whose lengths indicate the absolute values of principal stresses in the respective triangles.

3.6. Simulated locations of faults

Fault Formation mainly depends on the layer properties of rock, especially cohesion and angle of internal friction, and also the imposed convergent displacement.   The required physical properties of rock in our simulation are listed in Table 3.   Under the Mohr-Coulomb failure criterion concept, twenty experiments have been performed for models A and B with different combinations of convergent displacement *e.g.* 25 m, 30 m, 50 m, 75 m, 100 m, 125 m, 250 m, 300 m, 375 m and 500 m to examine faults.   All simulations are not presented here.   To show the characteristics of principal stresses within the failed elements, the experiments under convergent displacement 100 and 250 m have shown in Figs. 7A and B and Table 5.

Model A exhibits some failed elements in layers 2 and 5 with horizontal distribution of σ_1 which imply that thrust fault is dominant within the failed element (Figs. 7A1 and A2).   This is consistent with the stress distribution and fault development in the Nepal Himalaya (Alam and Hayashi, 2002).   Model B shows some of the failed elements in layer 2 and the upper part of layer 4 (Figs. 7B1 and B2).   Compressive σ_1 in layer 2 and 4 directed vertically which indicates that normal faults occur in these region.   Somewhere σ_1 is distributed horizontally and inclined direction in layers 4 and 2 of model B where thrusts and normal faults are also expected.   The results coincide with the focal mechanism solution for earthquakes in the Himalaya (Chandra, 1978).

4.   Discussions

4.1. How to decide layer properties

The geological profiles (Figs. 2A and B) in the north-western and central Himalaya have been modeled by the 2 D finite element method.   The basic assumptions of these models are relatively simple.   We simplify both profiles and divide them into five layers according to their regional tectonic divisions and specify the dominant rock types for each layer to reducce the complexity of calculations and to obtain the stress field for each model.   Five parameters of layer properties are Young's modulus, Poisson's ratio, density, cohesion and angle of internal friction.   The actual values of them are not well constrained; as a consequence, we have tested all the models with varying values of five constants in order to find the effect on the stress field.   The values which are finally decided are shown in Table 3.   Because several major structural units have different rheological properties, Young's modulus thus ranges from 40–80 GPa.   These parameters of rocks in each layer, presented in order of strength from high to low, are layer 1, layer 4, layer 3, layer 5, and layer 2.

4.2. How to decide convergent displacement

The displacement boundary condition simply corresponds to the convergence of the Eurasian plate relative to the Indian subplate. The Indian craton moves north-northeast at a rate of 44–61 mm/yr relative to Eurasia/Siberia (Armijo *et al.,* 1986;
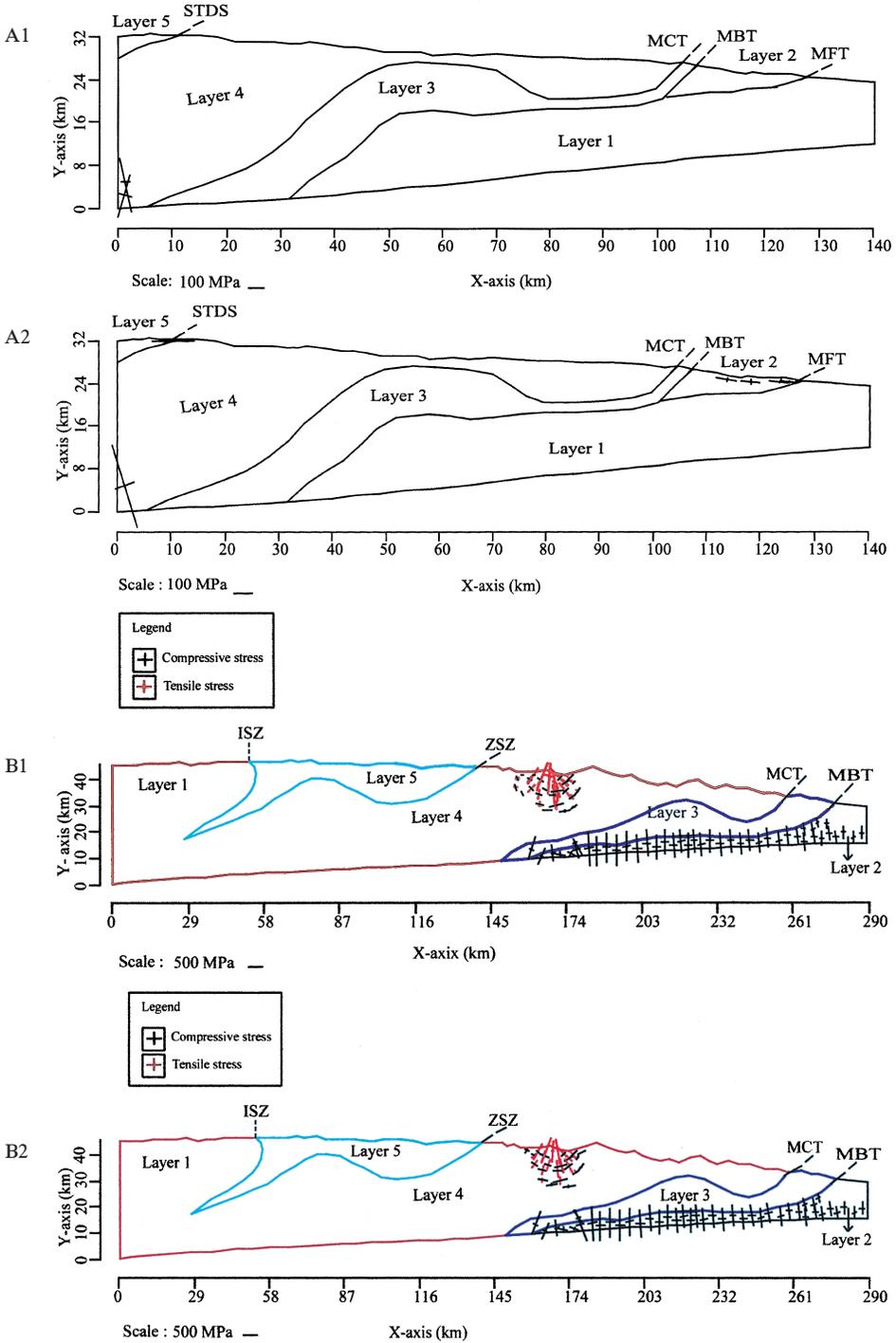
Fig. 7. Failure resulting from the stresses of models A1, A2, B1 and B2 after applying the concept of proximity to failure with 100 m and 250 m convergence displacements.

Table 5. Calculated failed elements and characteristics of principal stresses of models A and B under proximity to failure value.

Layer	Model A			Model B		
	Number of failed elements	State of stress	Direction of σ_1	Number of failed elements	State of stress	Direction of σ_1
Layer 1	No			No		
Layer 2	Some	Compressive	Horizontal	Some	Compressive	Vertical
Layer 3	No			No		
Layer 4	Some	Compressive	Inclined	Some	Tensile and compressive	Vertical, Horizontal and Inclined
Layer 5	Some	Compressive	Horizontal	No		

Bilham *et al.,* 1997). GPS geodesy has established the rate of India-Asia convergence at 54 ± 4 mm/yr. Only about 30% (*e.g.* 18 ± 2 mm/yr.) of the India-Asia convergence is absorbed across the Himalaya; thus, the average rate of accommodation derived on the basis of slip rates of great earthquakes is ~17 mm/yr. Recent GPS measurements along the Delhi-Malari and Delhi-Milam sections across the Kumaun Himalaya show that the Tethyan domain beyond the Great Himalaya is advancing southward at the rate of 18 to 20 mm/yr. On the basis of the convergence between India and Eurasia, we choose 25, 30, 50, 75, 100, 125, 250, 375, and 500 m as the displacement boundary conditions.

4.3. Relations between simulated results and tectonic features

Models contain five different geologic units which are separated by regional thrusts or discontinuities such as MFT, MBT, MCT, STDS, ZSZ and ISZ. The general features of the stress field and fault development are shown in Figs. 6A1 to 7B2. The stress fields of models A and B show nearly the same features all over the models (Figs. 6A and B). Within all layers, compressive σ_1 tends to be nearly vertical, and increases its area from shallow to deep.

In model A, MFT separates the Sub-Himalaya and Pre-Cambrian basement, and STDS marks the boundary between the Higher Himalaya and Tethys Himalaya. The present simulation shows that thrust faults are formed parallel along the real MFT and the real STDS as illustrated in Fig. 7A2 according to subduction of the Indian subplate under the Eurasian Plate. In model B, normal faults are formed beneath the MBT in the sub-Himalaya. The MBT is the major thrust in the Himalaya which was produced within the compressional wedge during the Cenozoic period (Mugnier *et al.,* 1994).

The present simulation shows the compressive σ_1 is directed vertically throughout the elongation of MBT as shown in Figs. 7B1 and B2.   We consider that the failed zones caused by the vertical σ_1 develop upward and the zones appear as normal faults on the surface.   Nakata (1989) states that the normal faults are observed at some places along the MBT which supports the existence of simulated normal faults along the MBT in model B (Figs. 7B1 and B2).

5.   Conclusions

(1)   Simulated normal faults below the MBT may be the explanation of the existence of normal faults reported by Nakata (1989).

(2)   Compressive stress is dominant over the modeled area but a few areas in the upper part of the Higher Himalaya are covered by tensile stress.

(3)   Magnitudes of σ_1 and σ_2 are higher in the deeper part than the upper part in both models.

(4)   Directions of principal stresses vary from layer to layer.   In general σ_1 is directed vertically and σ_2 horizontally in deeper regions, whereas they show reverse direction in the upper parts of all layers.

(5)   Most of the elements are failed in layer 2 (Sub-Himalaya), layer 5 (Tethys Himalaya) and in the upper part of layer 4 (Higher Himalaya).

These features allow us to infer that the direction and intensity of principle stresses are responsible for the formation of thrust and normal faults.   The formation of faults is intensely concentrated along Sub-Himalaya and upper part of layer 4.

Acknowledgments

References

Alam, M.M. and Hayashi, D. (2002): Stress distribution and fault development around the Nepal Himalaya by means of finite element method. Bull. Fac. Sci. Univ. Ryukyus, **73**, 15–54.

Anderson, E.M. (1951): The Dynamics of Faulting and Dyke Formation with Applications to Britain, 1st ed. London, Oliver, 206 p.

Arita, K., Shiraishi, K. and Hayashi, D. (1984): Geology of western Nepal and a Comparison with Kumaun, India. J. Fac., Sci., Hokkaido Univ., Ser. IV., **21 (1)**, 1–20.

Armijo, R., Tapponier, P., Mercier, J.L. and Tonglin, H. (1986): Quaternary extension in southern Tibet. J. Geophys. Res., **91**, 13803–13872.

Banghar, A.R. (1974): Focal mechanism of earthquakes in China, Mongolia, Russia, Nepal, Pakistan and Afganistan. Earthquake Notes, **45**, 1–11.

Bilham, R., Larson, K., Freymueller, J. and Project Idylhim members (1997): GPS measurements of present-day convergence across the Nepal Himalaya. Nature, **386**, 61–64.

Brunel, M. (1986): Ductile thrusting in the Himalayas: Shear sense criteria and stretching lineations. Tectonics, **5**, 247–265.

Chandra, U. (1978): Seismicity, earthquake mechanisms and tectonics along the Himalayan mountain range

and vicinity. Phys. Earth Planet. Inter., **16**, 109–131.

Dèzes, P. (1999): Tectonic and Metamorphic Evolution of the Central Himalayan Domain in Southeast Zanskar (Kashmir, India). Mém. Géol. (Lausanne), **32**, 149 p.

Gansser, A. (1964): Geology of the Himalayas. London, Interscience Publ., 289 p.

Hayashi, D. and Kizaki, K. (1972): Numerical analysis on migmatite dome with special reference to the finite element method. J. Geol. Soc. Jpn., **78**, 677–686.

Hayashi, D., Fuji, Y., Yoneshiro, T. and Kizaki, K. (1984): Geology of Karnali-Bheri region, west Nepal. J. Nepal Geol. Soc., **4**, 29–40.

Kano, T. (1984): Occurrence of augen gneisses in the Nepal Himalayas. J. Nepal Geol. Soc., **4**, Spec. Issue, 121–139.

Le Fort, P. (1975): Himalayas: the collided range. Present knowledge of the continental Arc. Am. J. Sci., **275**, 1–44.

Melosh, H. J. and Williams, C.A., Jr. (1989): Mechanics of graben formation in crustal rocks: a finite element analysis. J. Geophys. Res., **94**, 13961–13973.

Mugnier, J.L., Mascle, G. and Faucher, T. (1994): La structure des Siwaliks de l'ouest du Nepal: Un prisme d'accretion intracontinental. Bull. Soc. Geol. Fr., **163**, 585–595.

Nakata, T. (1989): Active faults of the Himalaya of India and Nepal. Spec. Pap. Geol. Soc. Am., **232**, 243–264.

Ni, J. and Barazangi, M. (1984): Seismotectonics of the Himalayan collision zone; geometry of the underthrusting Indian plate beneath the Himalaya. J. Geophys. Res., **89**, 1147–1163.

Pandey, M.R., Tandukar, R.P., Avouac, J.P., Vergne, J. and Heritier, T. (1999): Seismo-tectonics of the Nepal Himalaya from a local seismic network. J. Asian Earth Sci., **17**, 703–712.

Sorkhabi, R.B. and Macfarlane, A. (1999): Himalaya and Tibet: Mountain roots to mountain tops. Geol. Surv. Am., Spec. Pap., **328**, 1–8.

Sydney, P. and Clark, J.R. (1966): Handbook of Physical Constants. Geol. Soc. Am., Mem., **97**.

Timoshenko, S.P. and Goodier, J.N. (1970): Theory of Elasticity, 3rd ed. London, McGraw-Hill, 567 p.

Verma, R.K. (1997): Paleomagnetism from parts of Tethys Himalaya, Indus Suture Zone, Ladakh and South Tibet: Implications for collision between Indian and Eurasian Plate. Himalaya Geol., **18**, 93–102.